Earthq Eng & Eng Vib (2020) 19: 499-513 **DOI**: https://doi.org/10.1007/s11803-020-0577-7

Effect of inertia nonlinearity on dynamic response of an asymmetric building equipped with tuned mass dampers

Hassan Rezazadeh[1†], Fereidoun Amini[1‡] and Majid Amin Afshar[2§]

1. *School of Civil Engineering, Iran University of Science and Technology, P.O. Box 16765-163, Tehran, Iran*

2. *Department of Technology and Engineering, Imam Khomeini International University Norouzian, P.O. Box 34149-16818, Qazvin, Iran*

Abstract: This study investigates the effect of nonlinear inertia on the dynamic response of an asymmetric building equipped with Tuned Mass Dampers (TMDs). In the field of structural engineering, many researchers have developed models to study the behavior of nonlinear TMDs, but the effect of nonlinear inertia has not received as much attention for asymmetric buildings. To consider nonlinear inertia, the equations of motion are derived in a local rotary coordinates system. The displacements and rotations of the modeled building and TMDs are defined by five-degree-of-freedom (5-DOFs). The equations of motion are derived by using the Lagrangian method. Also in the proposed nonlinear model, the equations of motion are different from a conventional linear model. In order to compare the response of the proposed nonlinear model and a conventional linear model, numerical examples are presented and the response of the modeled buildings are derived under harmonic and earthquake excitations. It is shown that if the nonlinear inertia is considered, the response of the modeled structures changes and the conventional linear approach cannot adequately model the dynamic behavior of the asymmetric buildings which are equipped with TMDs.

Keywords: Nonlinear inertia; tuned mass damper; asymmetric buildings; harmonic excitation; seismic excitation

1 Introduction

A tuned mass damper (TMD) is a moving mass which is connected to the primary structure by springs and dampers (Viet and Nghi, 2014). The application of a TMD as a device to suppress the vibration of dynamic systems was first proposed by Frahm (Hsiao *et al.*, 2005). Since then, many researchers have investigated the effectiveness of linear TMDs to control the vibration of linear structures (Guo *et al.*, 2012). However, many important characteristics of a dynamic system can only be modeled by nonlinear governing equations. Moreover, there is a wide range of important phenomena that are nonlinear (Nayfeh, 2000).

Many researchers have studied the nonlinear behavior of TMDs in mechanical and structural systems. Alexander and Schilder (2009) studied the behavior of a nonlinear TMD, which was modeled as a two-degree-of-freedom system with cubic nonlinearity. In this study, the nonlinearity was physically derived from a geometric configuration of two pairs of springs. Wang (2011) proposed a new type of nonlinear TMD in order to improve its performance for machining chatter suppression. In this study, the nonlinear TMD was equipped with an additional series friction-spring element. Viet and Nghi (2014) considered a nonlinear single-mass two-frequency pendulum TMD to reduce horizontal vibration. Li and Cui (2017) studied the control performance of a TMD when nonlinear behavior caused by nonlinear spring stiffness is taken into account for practical application. Djemal *et al.* (2015) studied the nonlinear behavior of TMD, which was modeled as a two-degree-of-freedom system. In this study, the jump phenomenon of the nonlinear TMD was experimentally validated. Eason *et al.* (2015) studied the response attenuation of a linear primary structure (PS)-nonlinear tuned mass damper (NTMD) dynamic system with and without an adjustable-length pendulum tuned mass damper by using numerical and experimental methods.

On the other hand, several researchers have studied the effects of inertia nonlinearity on the behavior of nonlinear mechanical systems. Mayet and Ulbrich (2015) studied the nonlinear detuning of a centrifugal pendulum vibration absorber. Mamandi *et al*. (2010) studied the nonlinear behavior of an inclined beam subjected to a moving load. Hosseini and Khadem (2009) studied the free vibration of a rotating shaft with nonlinearities in curvature and inertia. Also in the field of the structural engineering, Amin Afshar and Aghaei Pour (2016) studied the inertia nonlinearity in irregular-plan isolated structures under seismic excitations.

Among the papers dealing with modeling nonlinear

Correspondence to: Fereidoun Amini, School of Civil Engineering, Iran University of Science and Technology, P.O. Box 16765-163, Tehran, Iran
Tel: +98-21-77240332; Fax: +98-21-77240398
E-mail: famini@iust.ac.ir
[†]Research Assistant; [‡]Professor; [§]Assistant Professor

Received December 11, 2017; **Accepted** September 29, 2019

TMD, very little attention has been given to inertia nonlinearity due to torsional-lateral coupling. However, if inertia nonlinearity is considered in an asymmetric building, the dynamic response of the building may change (Amini and Amin Afshar, 2011). Also, phenomena such as saturation, jump and energy transfer between modes can take place (Amini and Amin Afshar, 2011).

In this study, five degrees-of-freedom (5-DOFs) are defined to model the behavior of an asymmetric single story building equipped with TMDs. In the novel nonlinear approach, unlike conventional linear models, the inertia nonlinearity is not ignored. To consider the inertia nonlinearity in the equations of motion, the structure properties such as stiffness and damping are defined in a local rotary system of coordinates. The nonlinear equations of motion are also derived in a local rotary system of coordinates. However, in the conventional linear approach, the equations of motion are considered in a fixed global system of coordinates and the structure properties such as stiffness and damping are defined in the directions of the fixed axes.

The goal of this study is to show the weakness of the conventional linear approach to model the dynamic behavior of a single-story asymmetric building equipped with TMDs. In addition, a new approach is presented to model the dynamic behavior of an asymmetric building equipped with TMDs. By using a novel nonlinear approach proposed herein, the equations of motion will become quite different with the conventional linear approach. Also, if the inertia nonlinearity is considered, the response of the modeled structures may change under harmonic and seismic excitations.

This paper is organized as follows. In Section 2, the nonlinear equations of motion are derived and these equations are compared with conventional linear equations. In Section 3, the response of the modeled buildings is derived under harmonic excitations and the response of the linear and nonlinear models are compared. The response of the modeled buildings is also derived under seismic excitation. Conclusions are presented in Section 4.

2 Equations of motion

As shown in Fig. 1, a single-story asymmetric building is equipped with TMDs. It is assumed that the floor diaphragm is rigid. Moreover, the floor center of mass is denoted by $C.M_S$ and the story center of stiffness is represented by $C.R_S$. To consider the inertia nonlinearity, two coordinates systems are defined (see Fig. 2(b)). The first coordinates system is the local rotary *xyz* system, which is located on the base of the building and rotates by an angle θ. The second system is the global *XYZ* coordinates system, which is fixed on the ground.

The parameter e_x, denotes the eccentricity between the floor center of mass and story center of stiffness. This parameter can be calculated by

$$e_x = \frac{\sum_{j=1}^{N} x_{js} k_{yjs}}{\sum_{j=1}^{N} k_{yjs}} \tag{1}$$

where k_{yjs} denotes the stiffness of the *j*th resisting element in the y direction. The parameter x_{js} represents the *x*-coordinate of *j*th resisting element in the *y* direction.

Note that in this study, only the *x* direction eccentricity is considered. Trombetti and Conte (2005) verified that for a torsionally coupled one-story system, one of the mode shapes is purely translational. In this study and for each building, the *x* axis represents the mode shape which is purely translational (see Fig. 4(b)).

As seen in Fig. 2(a), in the conventional linear approach, the stiffness and damping parameters of the building and TMDs are defined in the global *XYZ* coordinates system. However, in the novel nonlinear approach, the stiffness and damping of the building and TMDs are defined in the local rotary coordinates system (see Fig. 2(b)).

The Lagrangian method is used here to derive the equations of motion. Based on the Lagrangian method, the motion equations in the local and global coordinates system can be derived by (Amini and Amin Afshar, 2011)

$$F_{qi} = \frac{\mathrm{d}}{\mathrm{d}t}\left(\frac{\partial L}{\partial \dot{q}_i}\right) - \frac{\partial L}{\partial q_i} \tag{2}$$

where q_i are the coordinates of the five degrees-of-freedom system in the global coordinates system (u_{Xs}, u_{Ys}, θ, u_{XT}, u_{YT}.) and the local one (u_{xs}, u_{ys}, θ, u_{xT}, u_{yT}). The variables u_{xs} and u_{ys} are the displacements of the floor center of mass in the *x* and *y* directions. Moreover, θ is the rotation of the one-story building about the *z* axis. Also u_{xT} and u_{yT} are the displacements of the TMDs in the *x* and *y* directions (see Fig. 3). In Eq. (2), F_{qi} are the external non-conservative forces such as

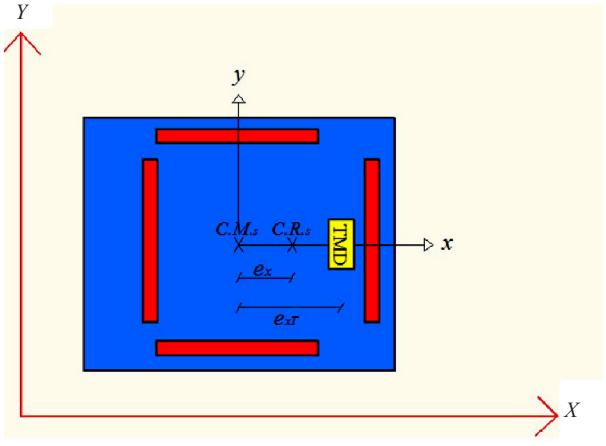

Fig. 1 Plan of the one-story building equipped with TMDs; : structure elements (beams and columns)

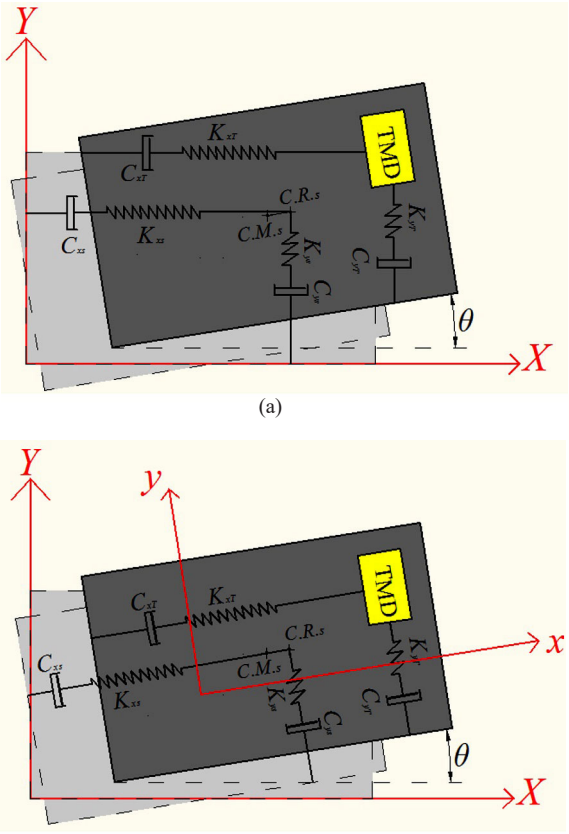

Fig. 2 Stiffness and damping parameters defined (a) in the global *XYZ* coordinates system and (b) in the local *xyz* coordinates system

excitation and damping forces and the parameter L is defined by (Amini and Amin Afshar, 2011)

$$L = T - V \tag{3}$$

where V is the potential energy which is stored in the resisting elements of the building and TMDs, also T is the total kinetic energy of the system (Amin Afshar and Aghaei Pour, 2016). The parameter V can be calculated by local DOFs as follows (Amini and Amin Afshar, 2011):

$$V = \frac{1}{2}\Big[K_{xs}u_{xs}^2 + K_{ys}(u_{ys} + e_x\theta)^2 + K_{\theta Rs}\theta^2 + K_{xT}(u_{xT} - u_{xs})^2 + K_{yT}(u_{yT} - u_{ys} - e_{xT}\theta)^2\Big] \tag{4}$$

Also, the value of V can be calculated by global DOFs by (Amini and Amin Afshar, 2011):

$$V = \frac{1}{2}\Big[K_{xs}u_{Xs}^2 + K_{ys}(u_{Ys} + e_x\theta)^2 + K_{\theta Rs}\theta^2 + K_{xT}(u_{XT} - u_{Xs})^2 + K_{yT}(u_{YT} - u_{Ys} - e_{xT}\theta)^2\Big] \tag{5}$$

Note that in Eqs. (4) and (5), the value of θ is assumed to be small. In Eqs. (4) and (5), the parameter $K_{\theta Rs}$ is the torsional stiffness of the one-story building and can be calculated by:

$$K_{\theta Rs} = \sum_{j=1}^{M} K_{xjs}y_{js}^2 + \sum_{j=1}^{N} K_{yjs}\left(x_{js} - e_x\right)^2 \tag{6}$$

where K_{xjs} is the stiffness of the jth element resisting in the x direction; and K_{yjs} is the stiffness of the jth element resisting in the y direction. In Eqs. (4) and (5), the parameters K_{ys} and K_{xs} are the total stiffness of the single-story building in the x and y directions. Moreover, in Eqs. (4) and (5), the parameters K_{xT} and K_{yT} are the stiffness of the springs which are connected to the TMDs in the x and y directions.

In Eq. (3) , the parameter T can be calculated by global DOFs as follows:

$$T = \frac{1}{2}\left[m_s\left(\frac{\mathrm{d}u_{Xs}}{\mathrm{d}t}\right)^2 + m_s\left(\frac{\mathrm{d}u_{Ys}}{\mathrm{d}t}\right)^2 + m_s r_s^2\left(\frac{\mathrm{d}\theta}{\mathrm{d}t}\right)^{22} + m_T\left(\frac{\mathrm{d}u_{XT}}{\mathrm{d}t}\right)^2 + m_T\left(\frac{\mathrm{d}u_{YT}}{\mathrm{d}t}\right)\right] \tag{7}$$

In the above equations, the parameters m_s and m_T are the total mass of the one-story building and TMDs, and r_s is the gyration radius of the floor about the floor center of mass. Note that in this research, TMDs have been considered as a lumped mass.

The relationship between global variables and local ones can be expressed as

$$\begin{bmatrix} u_{Xs} \\ u_{Ys} \\ \theta \\ u_{XT} \\ u_{YT} \end{bmatrix} = \begin{bmatrix} \cos\theta & -\sin\theta & 0 & 0 & 0 \\ \sin\theta & \cos\theta & 0 & 0 & 0 \\ 0 & 0 & 1 & 0 & 0 \\ 0 & 0 & 0 & \cos\theta & -\sin\theta \\ 0 & 0 & 0 & \sin\theta & \cos\theta \end{bmatrix} \begin{bmatrix} u_{xs} \\ u_{ys} \\ \theta \\ u_{xT} \\ u_{yT} \end{bmatrix} \tag{8}$$

where U_{Xg} and U_{Yg} are the displacements of the ground in the X and Y directions.

The dynamic equations of motion can be derived in two different forms. The first form is the conventional linear form and the second is the nonlinear form which is proposed herein. In Eq. (4), the potential energy is calculated in the local coordinates system and the proposed nonlinear equations can be derived. Also in Eq. (5) , the potential energy is calculated in the global coordinates system and conventional linear equations of motion can be derived.

The dynamic equations of motion can be derived by substituting the potential and kinetic energy in Eqs. (3) and (2). In the conventional approach, as seen in

Fig. 2(a), the damping and stiffness parameters are defined in the global *XYZ* coordinates system. Also in Fig. 2(b), the damping and stiffness parameters are defined in the local coordinates system.

In order to express the equations of motion in terms of non-dimensional parameters, these parameters are defined:

$$\omega_{xs}=\sqrt{\frac{K_{xs}}{m_s}},\ \omega_{ys}=\sqrt{\frac{K_{ys}}{m_s}},\ \omega_{\theta Rs}=\sqrt{\frac{K_{\theta Rs}}{m_s r_s^2}},$$
$$\omega_{xT}=\sqrt{\frac{K_{xT}}{m_T}},\ \omega_{yT}=\sqrt{\frac{K_{yT}}{m_T}} \tag{9}$$

$$\xi_{xs}=\frac{C_{xs}}{2m_s\omega_{xs}},\ \xi_{ys}=\frac{C_{ys}}{2m_s\omega_{ys}},\ \xi_{\theta Rs}=\frac{C_{\theta Rs}}{2m_s r^2\omega_{\theta s}},$$
$$\xi_{xT}=\frac{C_{xT}}{2m_T\omega_{xT}},\ \xi_{yT}=\frac{C_{yT}}{2m_T\omega_{yT}} \tag{10}$$

where $\omega_{\theta s}$ is defined by

$$\omega_{\theta s}=\sqrt{\frac{K_{\theta Rs}+K_{ys}e_x^2}{m_s r_s^2}} \tag{11}$$

In the above equations, C_{xs}, C_{ys} and $C_{\theta Rs}$ are damping coefficients of the one-story building, and C_{xT} and C_{yT} are the damping coefficients of the TMDs (see Fig. 2).

As previously mentioned, based on the Lagrangian method, the dynamic equations of motion in conventional linear form can be expressed as

$$\frac{\ddot{u}_{Xs}}{r_s}+\left(2\xi_{xs}\omega_{xs}+\frac{2}{\bar{m}}\xi_{xT}\omega_{xT}\right)\frac{\dot{u}_{Xs}}{r_s}+\left(\omega_{xs}^2+\frac{1}{\bar{m}}\omega_{xT}^2\right)\frac{u_{Xs}}{r_s}-$$
$$\frac{2}{\bar{m}}\xi_{xT}\omega_{xT}\frac{\dot{u}_{XT}}{r_s}-\frac{1}{\bar{m}}\omega_{xT}^2\frac{u_{XT}}{r_s}=-\frac{\ddot{U}_{gX}}{r_s} \tag{12}$$

$$\frac{\ddot{u}_{Ys}}{r_s}+\left(2\xi_{ys}\omega_{ys}+\frac{2}{\bar{m}}\xi_{yT}\omega_{yT}\right)\frac{\dot{u}_{Ys}}{r_s}+\left(\omega_{ys}^2+\frac{1}{\bar{m}}\omega_{yT}^2\right)\frac{u_{Ys}}{r_s}+$$
$$\left(2\frac{e_x}{r_s}\xi_{ys}\omega_{ys}+\frac{2}{\bar{m}}\frac{e_{xT}}{r_s}\xi_{yT}\omega_{yT}\right)\dot{\theta}+\left(\frac{e_x}{r_s}\omega_{ys}^2+\frac{1}{\bar{m}}\frac{e_{xT}}{r_s}\omega_{yT}^2\right)\theta-$$
$$\frac{2}{\bar{m}}\xi_{yT}\omega_{yT}\frac{\dot{u}_{YT}}{r_s}-\frac{1}{\bar{m}}\omega_{yT}^2\frac{u_{YT}}{r_s}=-\frac{\ddot{U}_{gY}}{r_s} \tag{13}$$

$$\ddot{\theta}+2\xi_{\theta Rs}\omega_{\theta s}\dot{\theta}+\left(\omega_{\theta s}^2+\frac{1}{\bar{m}}\omega_{yT}^2\frac{e_{xT}^2}{r_s^2}\right)\theta+\left(2\xi_{ys}\omega_{ys}\frac{e_x}{r_s}+\frac{2}{\bar{m}}\xi_{yT}\omega_{yT}\frac{e_{xT}}{r_s}\right)\frac{\dot{u}_{Ys}}{r_s}$$
$$-\frac{2}{\bar{m}}\xi_{yT}\omega_{yT}\frac{e_x}{r_s}\frac{\dot{u}_{YT}}{r_s}+\left(\omega_{ys}^2\frac{e_x}{r_s}+\frac{1}{\bar{m}}\omega_{yT}^2\frac{e_{xT}}{r_s}\right)\frac{u_{Ys}}{r_s}-\frac{1}{\bar{m}}\omega_{yT}^2\frac{e_{xT}}{r_s}\frac{u_{YT}}{r_s}=0 \tag{14}$$

$$\frac{\ddot{u}_{XT}}{r_s}+2\xi_{xT}\omega_{xT}\frac{\dot{u}_{XT}}{r_s}+\omega_{xT}^2\frac{u_{XT}}{r_s}-$$
$$2\xi_{xT}\omega_{xT}\frac{\dot{u}_{Xs}}{r_s}-\omega_{xT}^2\frac{u_{Xs}}{r_s}=-\frac{\ddot{U}_{gX}}{r_s} \tag{15}$$

$$\frac{\ddot{u}_{YT}}{r_s}+2\xi_{yT}\omega_{yT}\frac{\dot{u}_{YT}}{r_s}+\omega_{yT}^2\frac{u_{YT}}{r_s}-2\xi_{yT}\omega_{yT}\frac{\dot{u}_{Ys}}{r_s}-$$
$$\omega_{xT}^2\frac{u_{Ys}}{r_s}-2\xi_{yT}\omega_{yT}\frac{e_{xT}}{r_s}\dot{\theta}-\omega_{xT}^2\frac{e_{xT}}{r_s}\theta=-\frac{\ddot{U}_{gY}}{r_s} \tag{16}$$

In Eqs. (12)-(14), the parameter $\bar{m}$ is defined by:

$$\bar{m}=\frac{m_s}{m_T} \tag{17}$$

In the novel approach which is proposed in this study, as shown in Fig. 2(b), the damping and stiffness parameters are defined in the local rotary *xyz* coordinates system. The potential energy is derived based on local quantities (u_{xs}, u_{xs}, θ, u_{xT} and u_{yT}). If the potential energy is derived based on local quantities and it is substituted in Eqs. (3) and (2), the dynamic equations of motion can be expressed as

$$\frac{\ddot{u}_{xs}}{r_s}+\left(2\xi_{xs}\omega_{xs}+\frac{2}{\bar{m}}\xi_{xT}\omega_{xT}\right)\frac{\dot{u}_{xs}}{r_s}+\left(\omega_{xs}^2+\frac{1}{\bar{m}}\omega_{xT}^2\right)\frac{u_{xs}}{r_s}-$$
$$\frac{2}{\bar{m}}\xi_{xT}\omega_{xT}\frac{\dot{u}_{xT}}{r_s}-\frac{1}{\bar{m}}\omega_{xT}^2\frac{u_{xT}}{r_s}=$$
$$-\frac{1}{r_s}\left(-2\dot{u}_{ys}\dot{\theta}-u_{ys}\ddot{\theta}-u_{xs}\dot{\theta}^2+\ddot{U}_{gX}\cos\theta+\ddot{U}_{gY}\sin\theta\right) \tag{18}$$

$$\frac{\ddot{u}_{ys}}{r_s}+\left(2\xi_{ys}\omega_{ys}+\frac{2}{\bar{m}}\xi_{yT}\omega_{yT}\right)\frac{\dot{u}_{ys}}{r_s}+\left(\omega_{ys}^2+\frac{1}{\bar{m}}\omega_{yT}^2\right)\frac{u_{ys}}{r_s}+$$
$$\left(2\frac{e_x}{r_s}\xi_{ys}\omega_{ys}+\frac{2}{\bar{m}}\frac{e_{xT}}{r_s}\xi_{yT}\omega_{yT}\right)\dot{\theta}+\left(\frac{e_x}{r_s}\omega_{ys}^2+\frac{1}{\bar{m}}\frac{e_{xT}}{r_s}\omega_{yT}^2\right)\theta-$$
$$\frac{2}{\bar{m}}\xi_{yT}\omega_{yT}\frac{\dot{u}_{yT}}{r_s}-\frac{1}{\bar{m}}\omega_{yT}^2\frac{u_{yT}}{r_s}=$$
$$-\frac{1}{r_s}\left(2\dot{u}_{xs}\dot{\theta}+u_{xs}\ddot{\theta}-u_{ys}\dot{\theta}^2-\ddot{U}_{gX}\sin\theta+\ddot{U}_{gY}\cos\theta\right) \tag{19}$$

$$\ddot{\theta}+2\xi_{\theta Rs}\omega_{\theta s}\dot{\theta}+\left(\omega_{\theta s}^2+\frac{1}{\bar{m}}\omega_{yT}^2\frac{e_{xT}^2}{r_s^2}\right)\theta+\left(2\xi_{ys}\omega_{ys}\frac{e_x}{r_s}+\frac{2}{\bar{m}}\xi_{yT}\omega_{yT}\frac{e_{xT}}{r_s}\right)\frac{\dot{u}_{ys}}{r_s}-\frac{2}{\bar{m}}\xi_{yT}\omega_{yT}\frac{e_x}{r_s}\frac{\dot{u}_{yT}}{r_s}+\left(\omega_{ys}^2\frac{e_x}{r_s}+\frac{1}{\bar{m}}\omega_{yT}^2\frac{e_{xT}}{r_s}\right)\frac{u_{ys}}{r_s}-\frac{1}{\bar{m}}\omega_{yT}^2\frac{e_{xT}}{r_s}\frac{u_{yT}}{r_s}=0 \tag{20}$$

$$\frac{\ddot{u}_{xT}}{r_s}+2\xi_{xT}\omega_{xT}\frac{\dot{u}_{xT}}{r_s}+\omega_{xT}^2\frac{u_{xs}}{r_s}-2\xi_{xT}\omega_{xT}\frac{\dot{u}_{xs}}{r_s}-\omega_{xT}^2\frac{u_{xs}}{r_s}=-\frac{1}{r_s}\left(-2\dot{u}_{yT}\dot{\theta}-u_{yT}\ddot{\theta}-u_{xT}\dot{\theta}^2+\ddot{U}_{gX}\cos\theta+\ddot{U}_{gY}\sin\theta\right) \tag{21}$$

$$\frac{\ddot{u}_{yT}}{r_s}+2\xi_{yT}\omega_{yT}\frac{\dot{u}_{yT}}{r_s}+\omega_{yT}^2\frac{u_{yT}}{r_s}-2\xi_{yT}\omega_{yT}\frac{\dot{u}_{ys}}{r_s}-\omega_{xT}^2\frac{u_{ys}}{r_s}-2\xi_{yT}\omega_{yT}\frac{e_{xT}}{r_s}\dot{\theta}-\omega_{xT}^2\frac{e_{xT}}{r_s}\theta=-\frac{1}{r_s}\left(2\dot{u}_{xT}\dot{\theta}+u_{xT}\ddot{\theta}-u_{yT}\dot{\theta}^2-\ddot{U}_{gX}\sin\theta+\ddot{U}_{gY}\cos\theta\right) \tag{22}$$

It is seen that the Eqs. (18)-(22) are different from Eqs. (12)-(16), and nonlinear terms are observed in Eqs. (18)-(22). In Eqs. (18)-(22), the terms $-2\dot{u}_{ys}\dot{\theta}$, $2\dot{u}_{xs}\dot{\theta}$, $-2\dot{u}_{yT}\dot{\theta}$ and $2\dot{u}_{xT}\dot{\theta}$ are the Coriolis components of the acceleration. The terms $-u_{ys}\ddot{\theta}$, $u_{xs}\ddot{\theta}$, $-u_{yT}\ddot{\theta}$ and $u_{xT}\ddot{\theta}$ denote the tangential components of acceleration and the terms $-u_{xs}\dot{\theta}^2$, $-u_{ys}\dot{\theta}^2$, $-u_{xT}\dot{\theta}^2$ and $-u_{yT}\dot{\theta}^2$ are centrifugal componen of the acceleration.

3 Numerical study

In order to compare the performance of the proposed nonlinear model with the conventional linear model, three types of structures are considered. The natural frequencies of the modeled structe shown in Table 1. The properties of the modeled structu listed in Table 2. In the modeled structures, the damping ratio is assumed to be 4%. Note that the modeled structures are different only in torsional stiffness ($K_{\theta Rs}$) and the other parameters of these structures such as mass, translational stiffness, damping and gyration radius are the same. Structure type 1 has the maximum torsional stiffness and structure type 3 has the minimum torsioffness. In Table 1, the parameters Ω_1 and Ω_3 are defined by

$$\Omega_1=\frac{\omega_1}{\omega_{x1}},\ \Omega_3=\frac{\omega_3}{\omega_{x1}} \tag{23}$$

In Table 1, parameters ω_1, ω_{x1}, ω_3, ω_{x2} and ω_5 are the natural circular frequencies of the modeled structures in the first five modes. The position of the rigid diaphragm in the three first natural mode shapes of

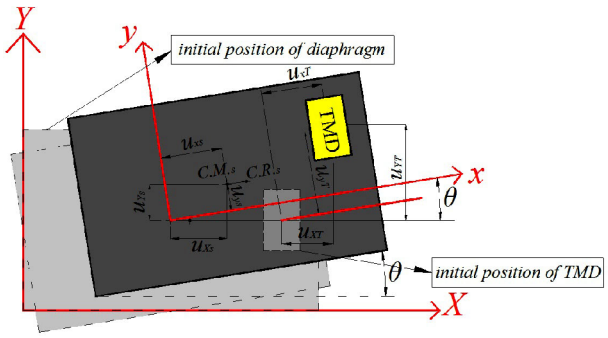

Fig. 3 Displacements of the structure and TMDs defined in the local and global coordinates systems

Table 1 Natural frequencies of the modeled structures

Structure type no.	ω_1 (rad/s)	ω_{x1} (rad/s)	ω_3 (rad/s)	ω_{x2} (rad/s)	ω_5 (rad/s)	Ω_1	Ω_3
1	9.44	10.46	11.97	14.34	16.92	0.90	1.14
2	6.67	10.46	11.08	14.34	15.80	0.64	1.06
3	5.24	10.46	10.98	14.34	15.63	0.50	1.05

Table 2 Properties of the modeled structures

structure type no.	ω_{xs} (rad/s)	ω_{ys} (rad/s)	$\omega_{\theta Rs}$ (rad/s)	ω_{xT} (rad/s)	ω_{yT} (rad/s)	e_x/r	e_{xT}/r	$\bar{m}$
1	12.24	12.24	12.75	12.25	12.25	0.5	0.5	10
2	12.24	12.24	7.78	12.25	12.25	0.5	0.5	10
3	12.24	12.24	5.99	12.25	12.25	0.5	0.5	10

the modeled structures is shown in Fig. 4.

The response of the modeled structures will be derived under harmonic excitations and earthquake excitations. The dynamic differential equations of motion have been solved by the SIMULINK toolbox of the MATLAB 8.0 solver package.

3.1 Structures response to harmonic excitation

As seen in Eqs. (18)-(22), the ground accelerations are denoted by $\ddot{U}_{gX}$ and $\ddot{U}_{gY}$ in the X and Y directions. In harmonic excitation, these parameters are selected to be:

$$\ddot{U}_{gX} = A\sin(\Omega_H \omega_{x1} t)\cos\beta \tag{24}$$

$$\ddot{U}_{gY} = A\sin(\Omega_H \omega_{x1} t)\sin\beta \tag{25}$$

where the parameter β is the excitation arrival angle with respect to the X direction. The variable Ω_H denotes the excitation frequency ratio. In the presented examples, the excitation arrival angle is assumed to be 60° with respect to the X direction, unless other values for β are mentioned.

The response of the linear and nonlinear models is compared in the time domain and frequency domain. The response of the structures in the frequency domain is derived by Fast Fourier Transform (FFT).

In this study, different values for β and A are selected to show the difference between the response of the linear and nonlinear models. In most of the presented numerical examples, the response of the linear and nonlinear models is identical at low amplitudes of excitation. Thus, the excitation amplitude is selected in a range to highlight the difference between the two models.

In Section 3.1.1 the parameters β and Ω_H are selected in a range so that the first mode of the structure is the dominant mode, and in Section 3.1.2, these parameters are selected to be in a range so that the second mode of the structure is the dominant mode. Note that if the parameter β is selected to be near zero, the second mode of the structure is the dominant mode and if β is near 90°, the first mode of the structure is the dominant mode.

3.1.1 Response of the structures under excitation with frequency ratio $\Omega_H = \Omega_1$

First, the response of the modeled structures are compared when the excitation frequency ratio is Ω_1. Figure 5 shows the response of structure type 1 under harmonic excitation. In this example, the variable A is selected to be 0.04 m/s^2. As seen in the figure, the response of structure type 1 in the linear and nonlinear models is the same. Moreover, the frequency content of the response is shown in Fig. 5(b). The dominant frequency of the response in the directions of X and Y, and θ is the frequency of the first mode (ω_1).

In structure type 1, if the amplitude of excitation is increased, or the excitation frequency is changed, the response of the linear and nonlinear models remain identical. Moreover, if the excitation arrival angle is changed, the response of linear and nonlinear models remains coincident. Thus, considering nonlinear terms in the motion equations of structure 1 is not important.

Time history and frequency content of structure type 3 are shown in Fig. 6. In this figure, the excitation amplitude is 0.04 m/s^2. In Fig. 6, it is seen that the response of the linear and nonlinear models are quite different. The frequency content of the X displacement shows that the nonlinear model has three peak points. One of the peak points is observed at frequency ratio Ω = 0, which means that the rigid diaphragm does not oscillate about its initial equilibrium position. Moreover, two other peak points occur at a frequency ratio of Ω=1.0 and Ω_1. As seen in Fig. 6(a), in initial steps of excitation, the response of the linear and nonlinear models are identical, but after the initial steps, the response of the linear and nonlinear models become quite different. In the nonlinear model, after the initial steps of excitation, the energy transfers from the mode with a frequency ratio of Ω_1 to the mode with a frequency ratio of Ω =1.0.

In Fig. 7, the time history and frequency content of

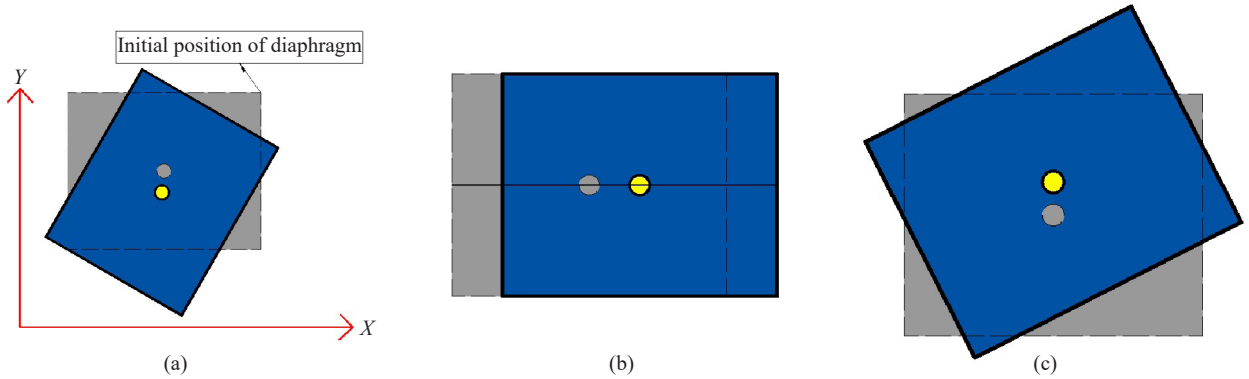

Fig. 4 Position of the rigid diaphragm in three first natural mode shapes of the modeled structures: (a) first natural mode with frequency of ω_1 and frequency ratio of Ω_1; (b) second natural mode with frequency of ω_{x1} and frequency ratio of Ω_1 = 1; (c) third natural mode; ● : initial position of the floor center of mass, ● : secondary position of the floor center of mass

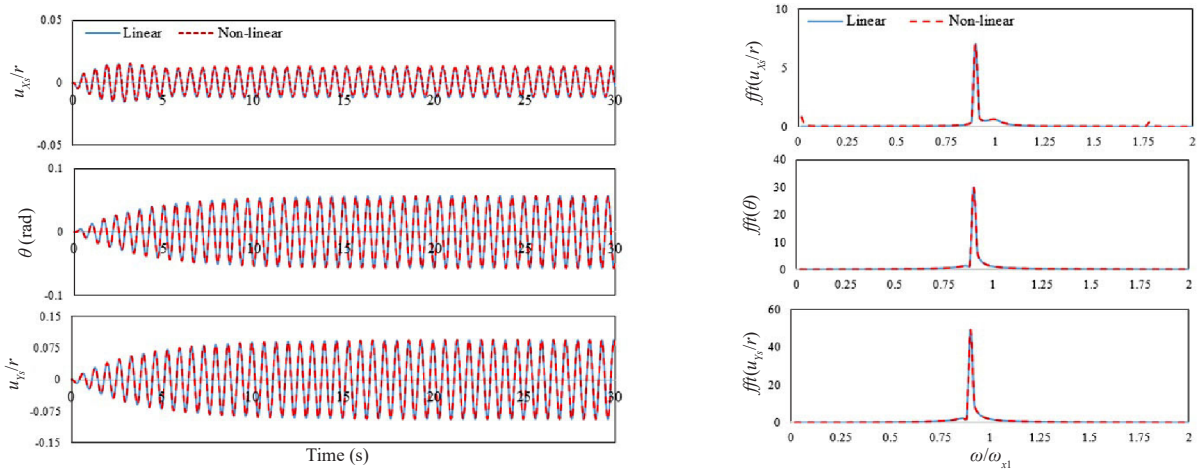

(a) (b)

Fig. 5 Response of structure type 1 under harmonic excitation with amplitude $A = 0.04$ m/s^2 and frequency ratio of $\Omega_H = \Omega_1$: (a) time history; (b) frequency content

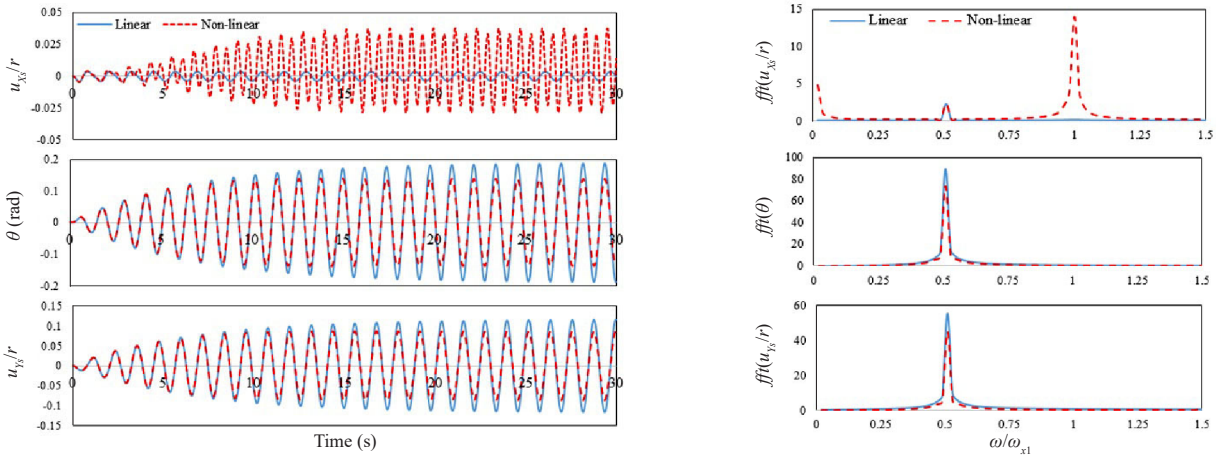

(a) (b)

Fig. 6 Response of structure type 3 under harmonic excitation with amplitude $A = 0.04$ m/s^2 and frequency ratio of $\Omega_H = \Omega_1$: (a) time history; (b) frequency content

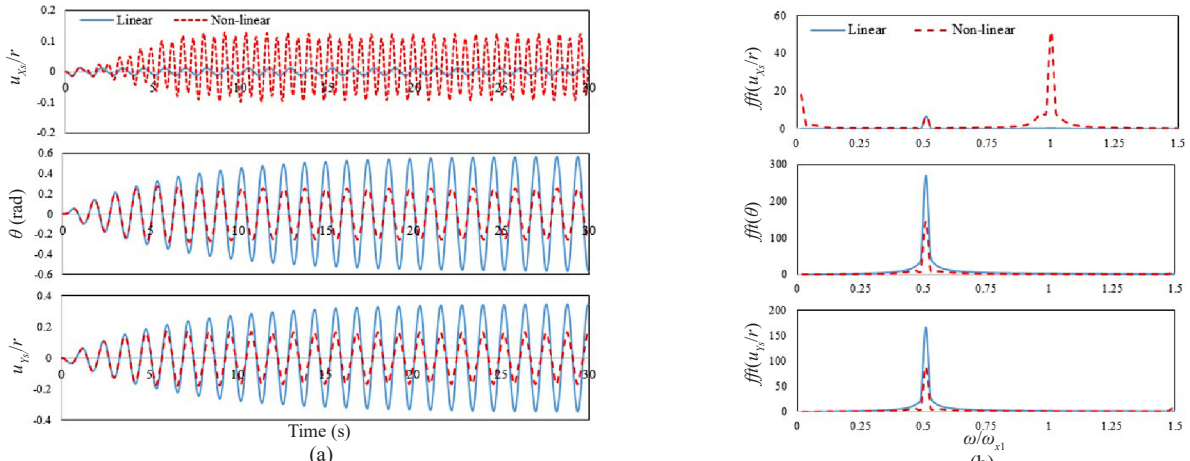

(a) (b)

Fig. 7 Response of structure type 3 under harmonic excitation with amplitude $A = 0.12$ m/s^2 and frequency ratio of $\Omega_H = \Omega_1$: (a) time history; (b) frequency content

structure type 3 are shown. In this figure, the excitation amplitude (A) is selected to be 0.12 m/s^2. By comparing the structure response in Figs. 6 and 7, it is concluded that if the excitation amplitude (A) is increased, the difference between the linear and nonlinear models becomes larger.

In Fig. 8, the response and frequency content of structure type 2 are shown. The excitation amplitude (A) is assumed to be 0.12 m/s^2. Again, it is seen that the response of linear and nonlinear models are not identical. The frequency content of the X displacement shows that the nonlinear model has three peak points. One peak point is observed at a frequency ratio of Ω = 0, and two more peak points occur at the frequency ratios of Ω_1 and $2\Omega_1$.

If Fig. 7 and Fig. 8 are compared, it is seen that the difference between the linear and nonlinear models is reduced for structure type 2. As previously mentioned, the torsional stiffness of structure type 2 is greater than structure type 3. Also in Fig. 7 and Fig. 8, energy transfer between modes is observed in the nonlinear model.

The time history and frequency content of structure type 2 is seen Fig. 9. In this example, the excitation amplitude (A) is 0.09 m/s^2. The parameter β is selected to be 90° . It is observed that in the linear model, the floor center of mass has no movement in the X direction. However, in the nonlinear model, the structure response is quite different as the floor center of mass oscillates in the X direction. The frequency response of the X displacement shows two peak points in the nonlinear model. One peak point is observed at the frequency ratio Ω = 0, which means that the structure does not oscillate about its initial equilibrium position in the X direction.

3.1.2 Response of the structure under excitation with frequency ratio Ω_H = 1.0

In Fig. 10, the response of structure type 3 is shown under harmonic excitation. The excitation amplitude (A) is selected to be 0.18 m/s^2, and the excitation arrival angle is assumed to be 2.86° (0.05 rad) with respect to the X axis (β = 0.05 rad). Note that if the parameter β

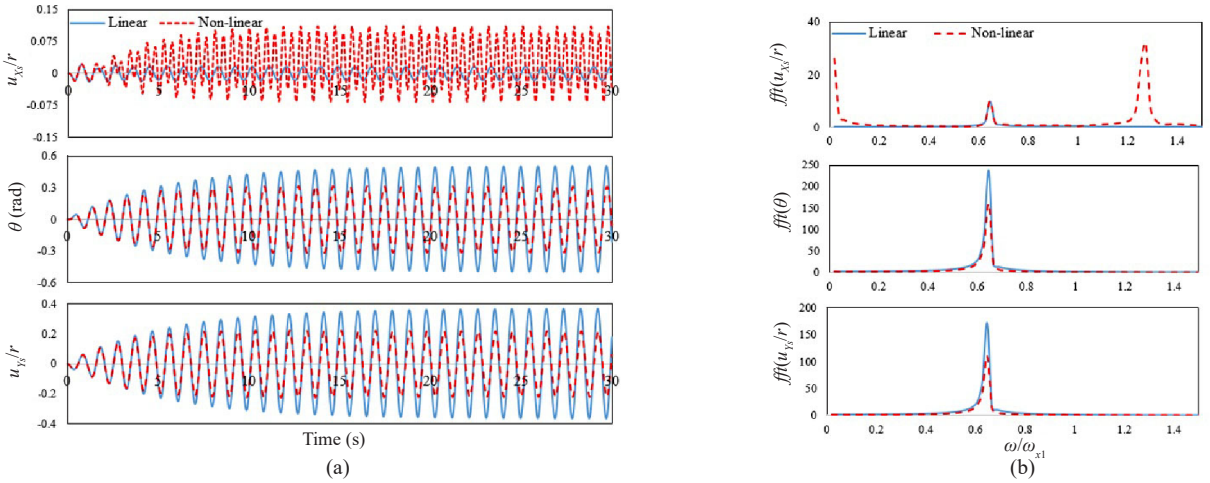

Fig. 8 Response of structure type 2 under harmonic excitation with amplitude A = 0.12 m/s^2 and frequency ratio of $\Omega_H = \Omega_1$: (a) time history; (b) frequency content

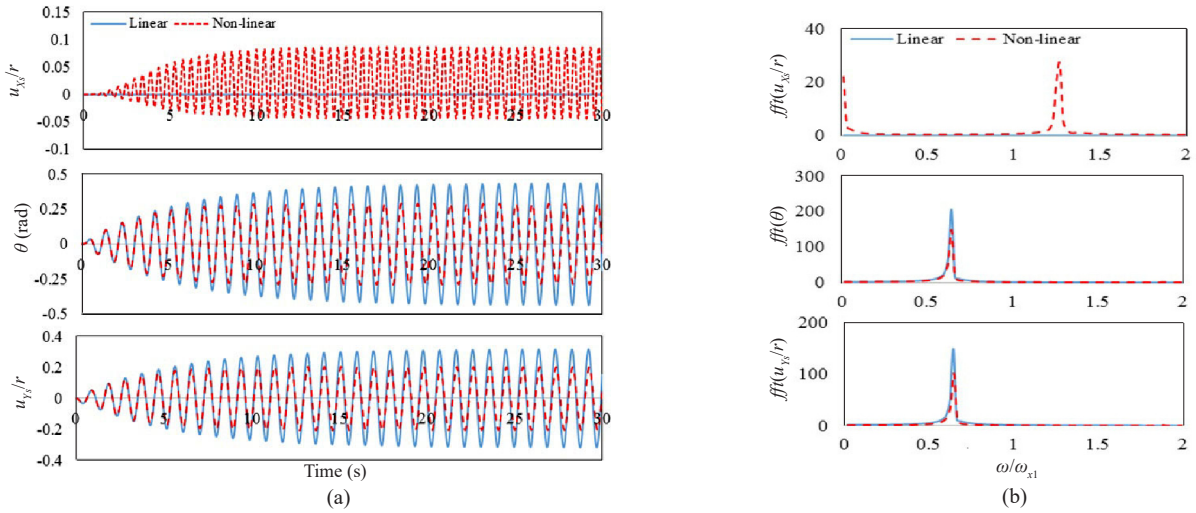

Fig. 9 Response of structure type 2 under harmonic excitation with amplitude A = 0.09 m/s^2, frequency ratio of $\Omega_H = \Omega_1$ and β = 90°: (a) time history; (b) frequency content

is equal to 0°, the response of the linear and nonlinear models becomes identical for all of the modeled structures. For example, the response of structure type 3 under harmonic excitation is shown in Fig. 11. In Fig. 11, the parameter β is selected to be 0° and the value of A is 0.18 m/s^2. Moreover, Ω_H is selected to be 1.0. It is seen that the response of the linear and nonlinear models is exactly the same. In this case, only the second mode of the structure is excited. As seen in Fig. 4(b), this mode is purely translational and in Fig. 11, the response of the structure is also purely translational and the torsional response of the structure is equal to zero. Moreover, in reality, it is not likely that the parameter β would be exactly equal to zero. For these reasons, in Fig. 10, a minor excitation arrival angle is selected which is near to zero ($\beta = 0.05$ rad $\approx 2.86°$).

As seen in Fig. 10, in the initial steps of excitation, the response of the linear and nonlinear models are identical. In the linear model, the amplitude of the response in the X direction increases in the initial steps of excitation and after that it reaches a certain constant value. However, in the nonlinear model, the amplitude of the response in the X direction increases first and after that it reaches a certain value and then the amplitude of response decreases. In the linear model, the amplitude of the response in the Y direction and θ remains near to zero through the excitation. However, in the nonlinear model, the response amplitude in the Y direction and θ increase after the initial steps of the excitation. In the frequency content of the X displacement, the main peak occurs at the frequency ratio of Ω = 1.0. In the linear model, this peak is greater than in the nonlinear model. When the energy, which is absorbed by the dominant mode in the X direction, reaches a certain amount, the saturation phenomenon occurs. When the saturation phenomenon takes place, the energy transfers from the dominant mode in the X direction to the mode with a frequency ratio of Ω_1; so the amplitude of the response in the X direction decreases and the amplitude of the response in the Y direction increases in the nonlinear

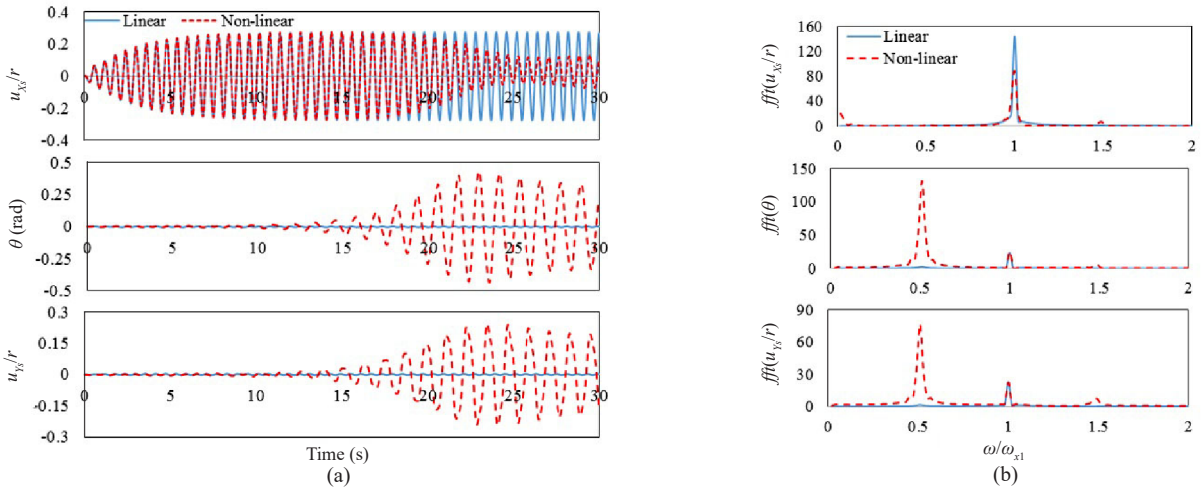

Fig. 10 Response of structure type 3 under harmonic excitation with amplitude A = 0.18 m/s^2, frequency ratio of Ω_H = 1.0 and β = 0.05 rad ≈ 2.86°: (a) time history; (b) frequency content

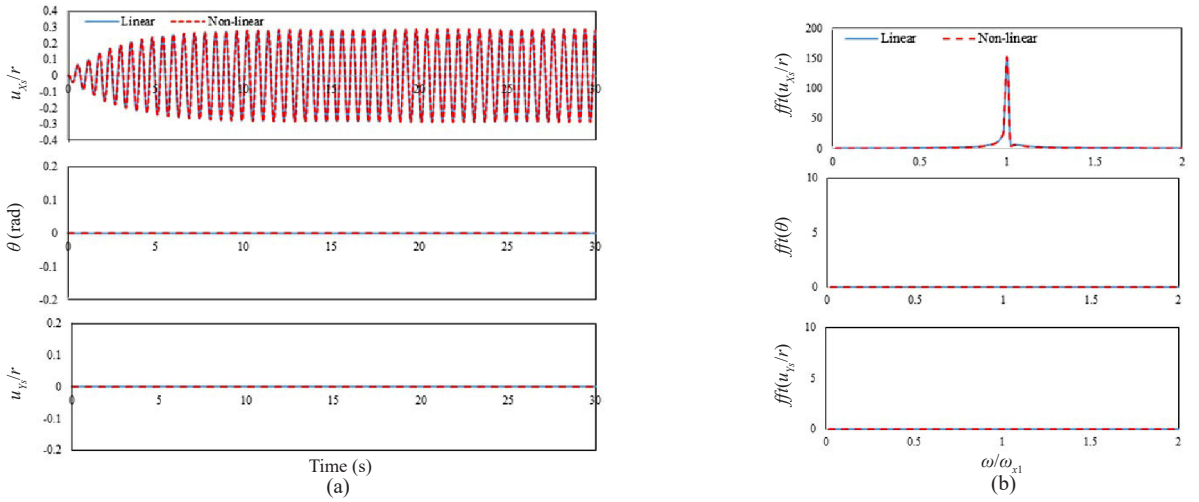

Fig. 11 Response of structure type 3 under harmonic excitation with amplitude A = 0.18 m/s^2, frequency ratio of Ω_H = 1.0 and β = 0°: (a) time history; (b) frequency content

model. Note that the mode with a frequency ratio of Ω_1 is the dominant mode in the response of the Y direction in the nonlinear model.

In Fig. 10(b), the frequency content of the X displacement shows that the nonlinear model has one small peak at a frequency ratio of $\Omega = 0$, which means that the floor center of mass does not oscillate about its initial equilibrium point. It is observed that after the saturation occurs, the floor center of mass oscillates around new position.

The response of structure type 2 in the time domain and frequency domain is seen in Fig. 12. The parameter β is 30°, and the parameter A is selected to be 0.2 m/s^2. It is observed that the response of linear and nonlinear models is not exactly the same, but are very similar and the difference between the two responses is negligible. In Fig. 12, the dominant mode of the structure is the second mode with a frequency ratio of Ω_{x1}. Here, unlike Fig. 10, the saturation phenomenon does not take place and the energy is not transferred between modes. Note that in structure types 3 and 2, the ratio between ω_{x1} and ω_1 is:

$$\frac{\omega_{x1}}{\omega_1} \approx 2.0 \tag{26}$$

$$\frac{\omega_{x1}}{\omega_1} \approx 1.57 \tag{27}$$

As seen in Eq. (26) for structure type 3, the ratio between ω_{x1} and ω_1 is 2:1. This ratio enables the structure to be more capable of saturation phenomenon. The saturation phenomenon can occur in structure type 2; however, it happens at higher amplitudes of excitation. In the next section, the maximum amplitude of the response in the linear and nonlinear models is compared.

3.1.3 Comparing the maximum response of the linear and nonlinear models under harmonic excitation

In Figs. 13-17 the maximum response of the linear

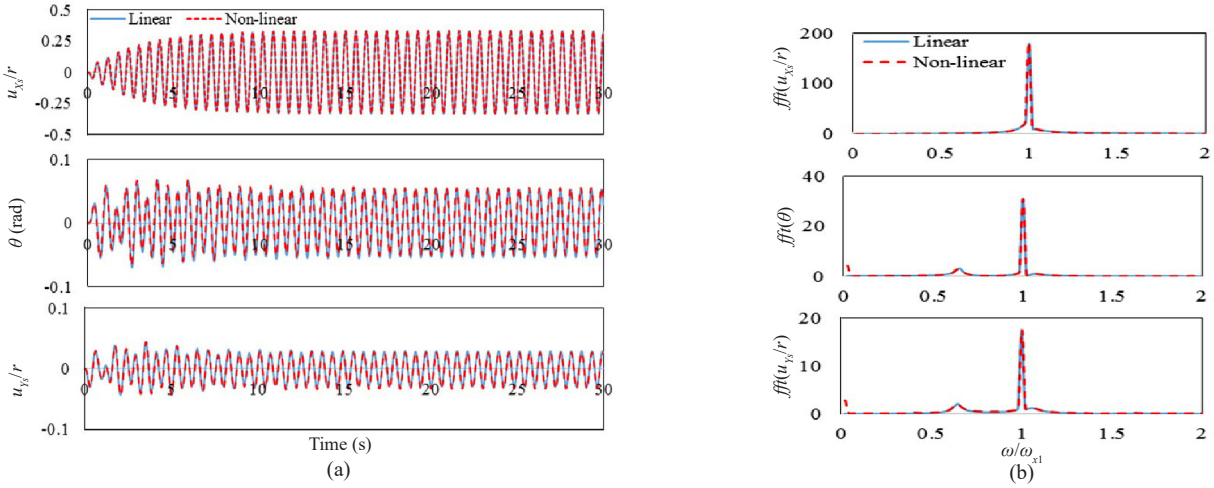

Fig. 12 Response of structure type 2 under harmonic excitation with amplitude A = 0.20 m/s^2, frequency ratio of Ω_H = 1.0 and β = 30°: (a) time history; (b) frequency content

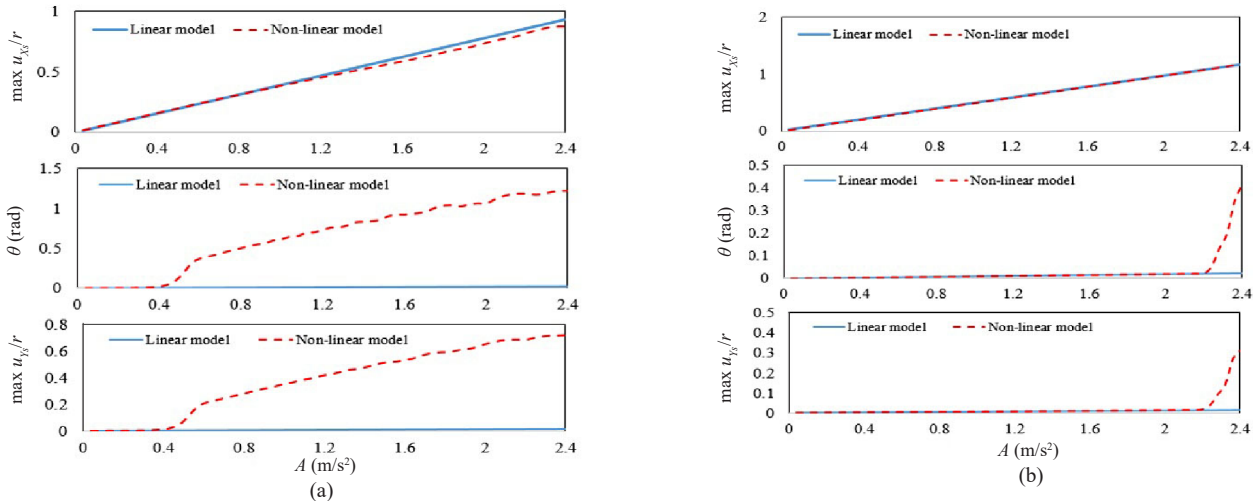

Fig. 13 Maximum response of the modeled structures under harmonic excitation with frequency ratio of Ω_H = 1.0 and β = 0.05 rad ≈ 2.86°: (a) type 3; (b) type 2

and nonlinear models are compared when the excitation amplitude (A) is increased. Note that in structure type 1, the maximum response of the linear and nonlinear models is identical. Thus, the comparison between linear and nonlinear models is not shown for structure type 1. Also, the parameter β is selected to be 0.05 rad (2.86°), 30°, 60° and 90°. If the parameter β is 0.05 rad (2.86°) or 30°, the second mode of the structure will be dominant mode. If the parameter β is 60° or 90°, the first mode of the structure will be dominant mode. It is seen that when the excitation amplitude increases, the difference between the maximum response of the linear and nonlinear models becomes greater. In Fig. 13 and 14, the parameter β is assumed to be 0.05 rad (2.86°) and 30° and the parameter Ω_H is selected to be 1.0. In Fig. 13(a) and structure type 3, the maximum response of the linear and nonlinear models are identical if the excitation amplitude (A) is less than 0.4 m/s^2. When the excitation amplitude becomes greater than 0.4 m/s^2, the maximum response of the linear and nonlinear models change (see Fig. 13(a)). In structure type 2, the maximum response of the linear and nonlinear models changes if the excitation amplitude becomes greater than 0.56 m/s^2 (see Fig. 13(b)). In Figs. 13 and 14, the maximum response of the linear and nonlinear models changes due to the saturation phenomenon. As was shown earlier, the saturation phenomenon occurs in structure type 3 when its second mode is the dominant one. The saturation phenomenon can also occur in structure type 2, where it occurs at higher amplitudes than in structure type 3. As previously mentioned, the ratio between ω_{x1} and ω_1 is 2:1 for structure type 3. This ratio enables structure type 3 to be more capable of saturation.

In Figs.15 and 16, the parameter Ω_H is selected to be equal to Ω_1, and the parameter β is selected to be 60° and 90°. It is seen that in both structure types 3 and 2, the

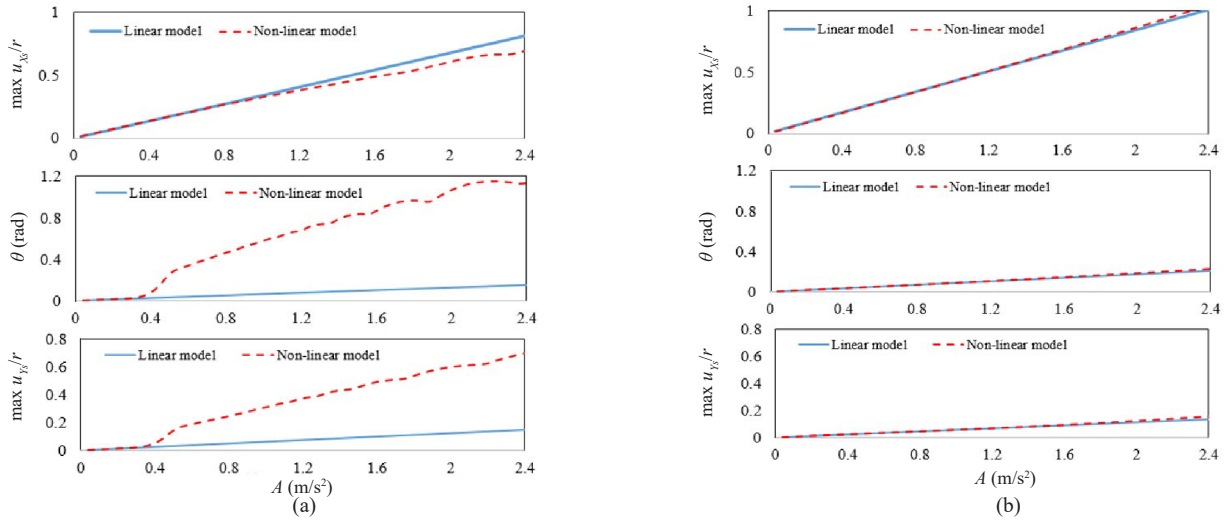

Fig. 14 Maximum response of the modeled structures under harmonic excitation with frequency ratio of Ω_H = 1.0 and β = 30°: (a) type 3; (b) type 2

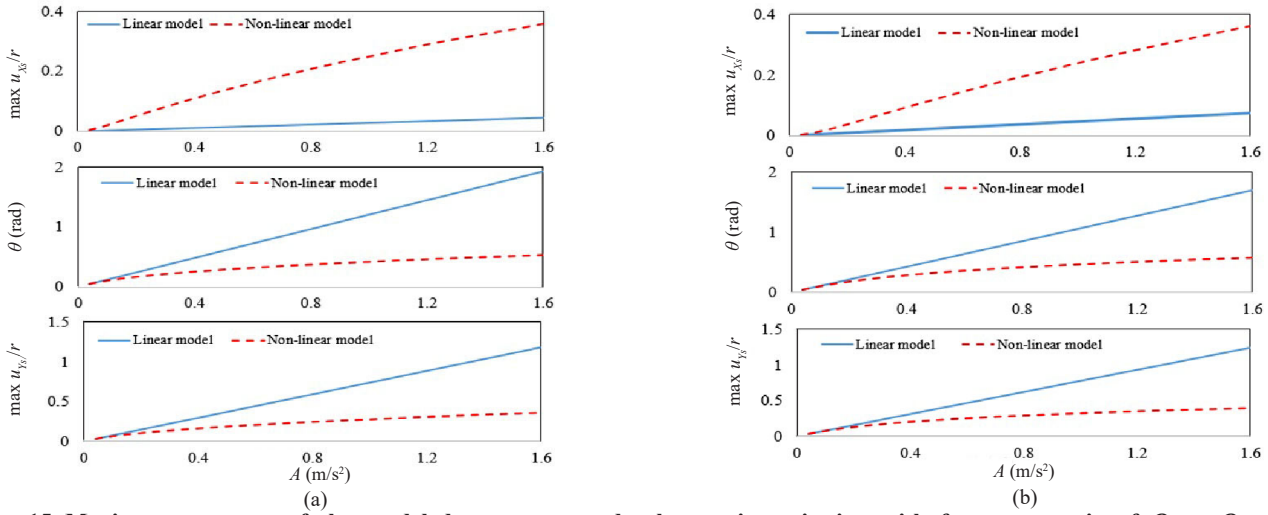

Fig. 15 Maximum response of the modeled structures under harmonic excitation with frequency ratio of Ω_H = Ω_1 and β = 60°: (a) type 3; (b) type 2

maximum response of the linear and nonlinear models are quite different. Unlike Figs. 13 and 14, the maximum response of the linear and nonlinear models is different even in the low amplitude of excitation.

3.2 Response to the seismic excitation

In this section, the response of the modeled structures is compared under seismic excitations. As seen in Fig. 17, two records from the Chi-Chi 1999 and 1940 El Centro earthquakes are selected to be applied to the modeled structures. In this section, the parameter β is selected to be 90° and 0.05 rad (≈ 2.86°). If the parameter β is 0.05 rad (≈ 2.86°), the translational mode of the structure is the dominant mode and if β is 90°, the first mode of the structure is the dominant mode. As previously mentioned, in most of the modeled structures, the response of the linear and nonlinear models is identical for low amplitudes of excitation. Thus, the maximum ground acceleration is selected in a range to show the difference between the response of the linear and nonlinear models.

Figure 18 shows the time and frequency response of structure type 3 under the Chi-Chi earthquake. The earthquake record is scaled, and its maximum acceleration is selected to be 0.4 g. β is selected to be 90°. It is seen that in the linear model, the response in the X direction remains zero throughout the excitation. However, in the nonlinear model, the response in the X direction is not zero. The maximum response in the Y direction and θ is greater in the linear model. The frequency content of the X displacement shows two peak points in the nonlinear model. One of the peak points is observed at the frequency ratio, $\Omega = 0$, which means that the floor center of mass has pure translation in the X direction. In the nonlinear model, it is observed that the energy transfers from the mode with a frequency ratio of Ω_1 to the mode with a frequency ratio of $\Omega = 1.0$.

In Fig. 19, the response of structure type 2 under El Centro excitation is shown. The parameter β is selected to be 90° and the maximum ground acceleration is 0.4 g. Again the energy transfer between modes is observed. In the frequency response of the X displacement, the main peak point occurs at a frequency ratio of $2\Omega_1$ for the nonlinear model. Another peak is seen in the frequency ratio of $\Omega = 1.0$. Moreover, one peak point is observed at the frequency ratio of $\Omega = 0$.

The response of structure type 3 under the El Centro earthquake is shown in Fig. 20. In this figure, the parameter β is 0.05 rad (2.86°). The maximum acceleration of the earthquake is selected to be 0.6 g. The response of the structure in the Y direction and θ is quite different in the linear and nonlinear models. However, the response of the linear and nonlinear models is very close to each other in the X direction. The frequency content of the Y displacement and θ shows that the main peak point occurs at a frequency ratio of Ω_1. In the nonlinear model, these peaks are greater than in the linear model.

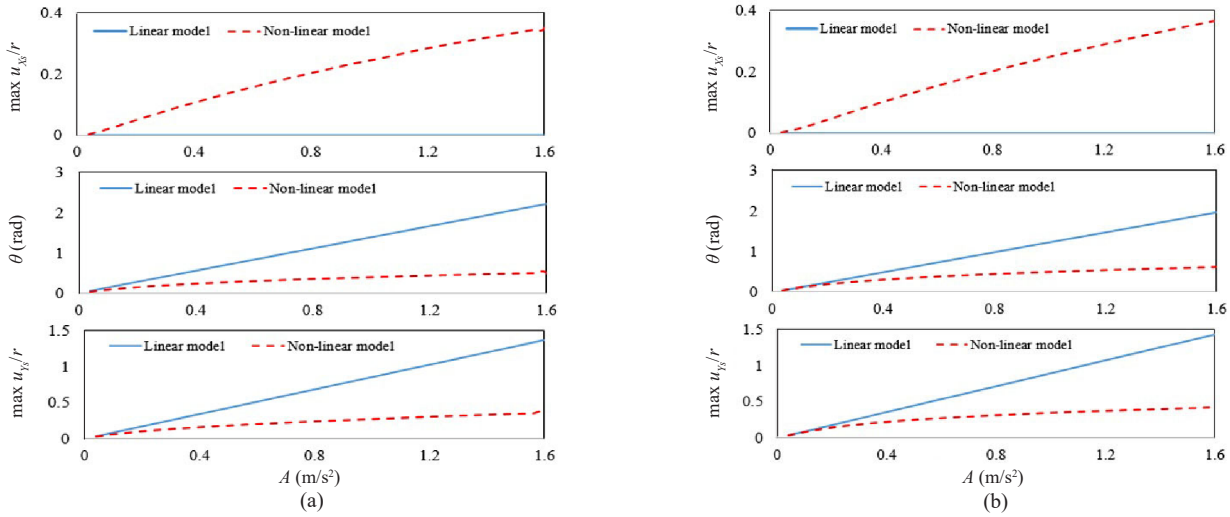

Fig. 16 Maximum response of the modeled structures under harmonic excitation with frequency ratio of $\Omega_H = \Omega_1$ and $\beta = 90°$: (a) type 3; (b) type 2

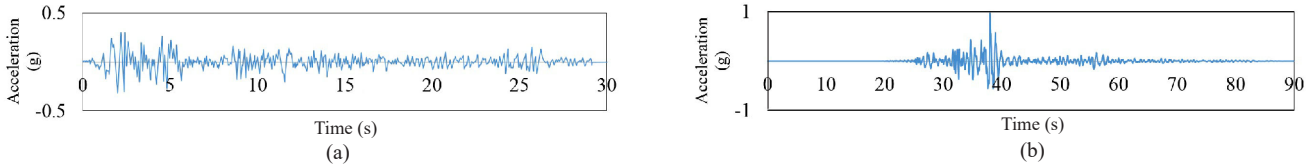

Fig. 17 Selected earthquakes accelerograms: (a) 1940 El Centro; (b) 1999 Chi-Chi

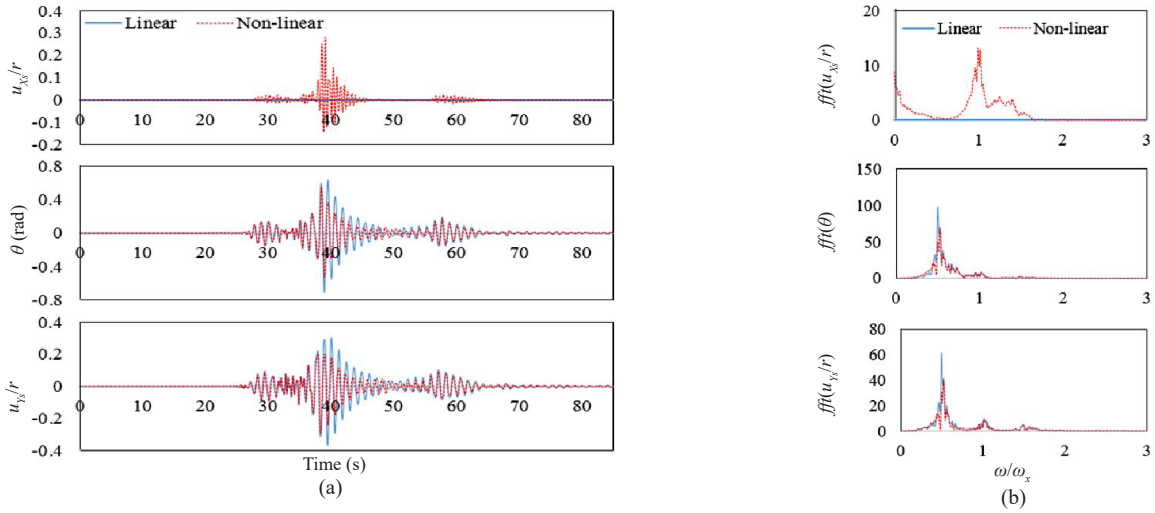

Fig. 18 Response of structure type 3 under Chi-Chi earthquake, $\beta = 90^\circ$, maximum acceleration of the ground is 0.4 g : (a) time history; (b) frequency content

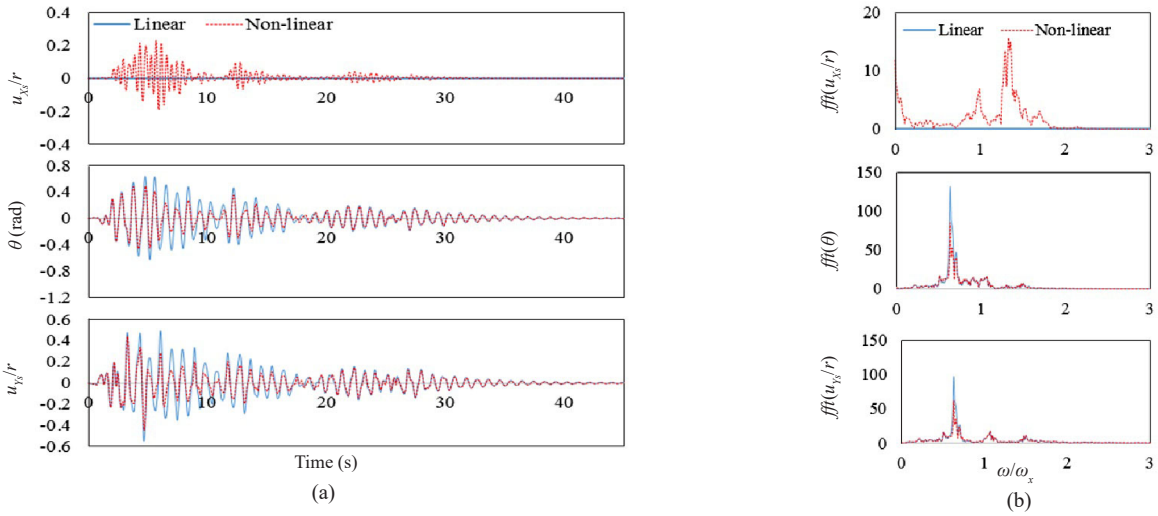

Fig. 19 Response of structure type 2 under El Centro earthquake, $\beta = 90^\circ$, maximum acceleration of the ground is 0.4 g (a) time history; (b) frequency content

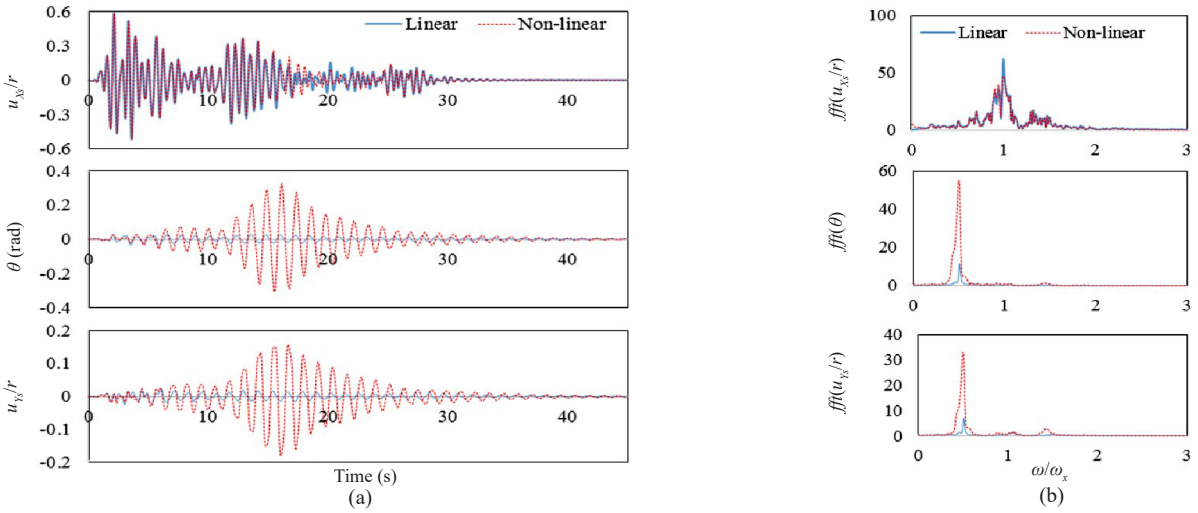

Fig. 20 Response of the structure type 3 under El Centro earthquake, $\beta = 0.05$ rad $\approx 2.86^\circ$, maximum acceleration of the ground is 0.6 g: (a) time history; (b) frequency content

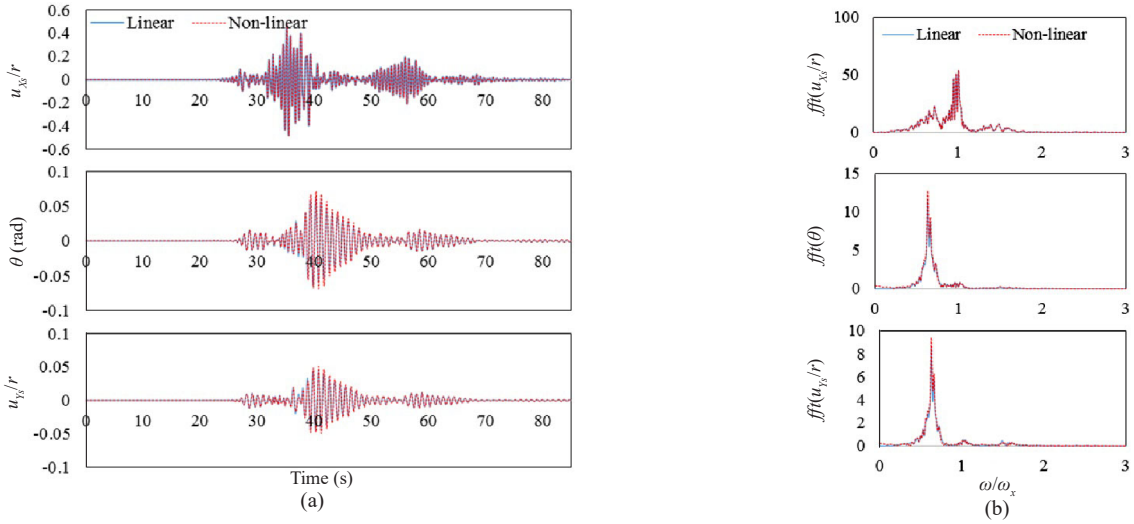

Fig. 21 Response of structure type 2 under Chi-Chi earthquake, β = 0.05 rad ≈ 2.86°, maximum acceleration of the ground is 0.6 g: (a) time history; (b) frequency content

The response of structure type 2 under the Chi-Chi earthquake excitation is shown in Fig. 21. In this figure, the parameter β is 0.05 rad (2.86°). The maximum acceleration of the earthquake is selected to be 0.6 g. It is seen that the response of the linear model is very close to the response of the nonlinear model and the difference between these two models can be ignored.

4 Summary and conclusions

In this study, the effect of nonlinear inertia on the dynamic behavior of asymmetric buildings equipped with TMDs was studied. The Lagrangian method was used to derive the nonlinear equations of motion. These nonlinear equations of motion were different from conventional linear equations. Three types of asymmetric structures were considered. Structure type 1 had maximum torsional stiffness and structure type 3 had minimum torsional stiffness. In the modeled structures, the first mode shape was torsional and the second mode shape was purely translational.

In structure type 1, the response of the linear and nonlinear models was the same and considering nonlinear inertia was not important.

In structure types 2 and 3, if the dominant mode of the structure was the torsional mode, the energy transfer phenomenon occurred between modes. The energy transfer took place even in low amplitudes of excitation. When the energy transfer between the modes occurred, the response of the linear and nonlinear models was different.

In structure types 2 and 3, if the dominant mode of the structure was the translational mode, the saturation phenomenon could occur. For these structures, if the saturation phenomenon occurred, the response of the linear and nonlinear models was different. In structure type 2, the saturation phenomenon could have only occurred in high amplitudes of excitation.

However, in structure type 3, the saturation phenomenon was possible even in low amplitude of excitation. For this reason, the response of the linear and nonlinear models was different, even in low amplitudes of excitation. In structure type 3, the ratio between the frequency of the first mode and second mode was selected to be 1:2 and structure type 3 was more capable of having the saturation phenomenon.

In structure types 3 and 2, the response of the linear and nonlinear models might be quite different even in low amplitudes of excitation. In these structures, if the nonlinear inertia was considered, phenomena such as saturation and energy transfer may take place. Also, if the amplitude of the excitation was increased, the difference between the response of the linear and nonlinear models was greater.

In structure types 3 and 2, considering the nonlinear inertia was essential and the conventional linear approach was unable to adequately model the behavior of these structures under seismic and harmonic excitations.

References

Alexander NA and Schilder F (2009), "Exploring the Performance of a Nonlinear Tuned Mass Damper," *Journal of Sound and Vibration*, **319**: 445–462.

Amin Afshar M and Aghaei Pour S (2016), "On Inertia Nonlinearity in Irregular-Plan Isolated Structures under Seismic Excitations," *Journal of Sound and Vibration*, **363**: 495–516.

Amini F and Amin Afshar M (2011), "Saturation in Asymmetric Structures under Internal Resonance," *Acta Mechanica*, **221**: 353–368.

Djemal F, Chaari F, Dion JL, Renaud F, Tawfiq I and Haddar M (2015), "Performance of a Nonlinear Dynamic

Vibration Absorbers," *Journal of Mechanics*, 1–9.

Eason RP, Sun C, Dick AJ and Nagarajaiah S (2015), "Steady-State Response Attenuation of a Linear Oscillator–Nonlinear Absorber System by Using an Adjustable-Length Pendulum in Series: Numerical and Experimental Results," *Journal of Sound and Vibration*, **344**: 332–344.

Guo W, Li HN, Liu GH and Yu ZW (2012), "A Simplified Optimization Strategy for Nonlinear Tuned Mass Damper in Structural Vibration Control," *Asian Journal of Control*, **14**(5): 1–11.

Hosseini SAA and Khadem SE (2009), "Free Vibrations Analysis of a Rotating Shaft with Nonlinearities in Curvature and Inertia," *Mechanism and Machine Theory*, **44**: 272–288.

Hsiao FH, Chen CW, Wu YH and Chiang WL (2005), "Fuzzy Controllers for Nonlinear Interconnected TMD Systems with External Force," *Journal of Chinese Institute of Engineers*, **28**(1): 175–181.

Li L and Cui P (2017), "Novel Design Approach of a Nonlinear Tuned Mass Damper with Duffing Stiffness," *Journal of Engineering Mechanics*, **143**(4).

Mamandi A, Kargarnovin MH and Younesian D (2010), "Nonlinear Dynamics of an Inclined Beam Subjected to a Moving Load," *Nonlinear Dynamics*, **60**: 277–293.

Mayet J and Ulbrich H (2015), "First-Order Optimal Linear and Nonlinear Detuning of Centrifugal Pendulum Vibration Absorbers," *Journal of Sound and Vibration*, **335**: 34–54.

Nayfeh AH (2000), *Nonlinear Interactions: Analytical, Computational, and Experimental Methods*, Wiley-Interscience, New York.

Trombetti TL and Conte JP (2005) "New Insight into and Simplified Approach to Seismic Analysis of Torsionally Coupled One-Story, Elastic Systems", *Journal of Sound and Vibration*, **286**: 265–312.

Viet LD and Nghi NB (2014), "On a Nonlinear Single-Mass Two-Frequency Pendulum Tuned Mass Damper to Reduce Horizontal Vibration," *Engineering Structures*, **81**: 175–180.

Wang M (2011), "Feasibility Study of Nonlinear Tuned Mass Damper for Machining Chatter Suppression," *Journal of Sound and Vibration*, **330**: 1917–1930.